mater.scichina.com link.springer.com

Published online 23 June 2020 | https://doi.org/10.1007/s40843-020-1356-3
Sci China Mater 2020, 63(8): 1570–1578

SPECIAL ISSUE: Optical Gain Materials towards Enhanced Light-Matter Interactions

Record high photoresponse observed in CdS-black phosphorous van der Waals heterojunction photodiode

Muhammad Zubair[†], Chenguang Zhu[†], Xingxia Sun[†], Huawei Liu, Biyuan Zheng, Jiali Yi, Xiaoli Zhu, Dong Li[*] and Anlian Pan[*]

ABSTRACT **Two-dimensional (2D) materials have recently received great attention for their atomic thin thickness and thus derived outstanding electrical, optical and optoelectronic properties. Moreover, the dangling-bond-free surfaces of 2D materials enable the direct integration of different materials with various properties through van der Waals (vdW) forces into vdW heterostructures, providing new opportunities for constructing new type devices with superior performances. In this study, we report the vertical assembly of n-type CdS and p-type BP into p-n junctions. The electrically tunable heterojunction device shows a high current rectifying ratio up to 8×10^3 at a low bias voltage range of ±1 V and an ideality factor of 1.5. More interestingly, the CdS/BP vdW heterojunction exhibits an ultra-high photoresponsivity up to 9.2×10^5 A W^{-1} and an ultra-high specific detectivity of 3.2×10^{13} Jones with a low bias voltage of 1.0 V, which is among the highest in the reported results of 2D heterostructures. While operated at a self-powered mode, the device also exhibits excellent photodetection performances with a high photoresponsivity of 0.27 A W^{-1} and a high external quantum efficiency of 76%. Time-resolved photoresponse characterizations indicate that the device possesses a fast response time of about 10 ms. The developed CdS/BP vdW heterojunctions will find potential applications in the next-generation nanoscale electronics and optoelectronics applications.**

Keywords: CdS/BP, van der Waals heterojunction, type tunable electrical properties, photovoltaic, self-driven photodetector

INTRODUCTION

The newly emerged two-dimensional (2D) layered materials, such as graphene [1,2], transition metal dichalcogenides (TMDs) [3–5] and black phosphorus (BP) [6], have been intensely investigated over the past few years due to their intriguing physical and structural properties [7–9], providing promising platforms for designing new semiconductor devices for diverse applications. The dangling-bond-free surfaces of 2D materials enable the creation of high-quality van der Waals (vdW) heterostructures with atomically sharp interfaces without being restricted by lattice mismatch as compared with conventional bulk semiconductor heterostructures [4,10,11], which offers complete degree of freedom in designing new artificial materials with novel properties. It has been proved that, in this way, 2D vdW p-n junctions, such as BP/ReS_2 [12], GaSe/WS_2 [13], WSe_2/SnS_2 [14], $MoTe_2$/MoS_2 [15], MoS_2/CdS [16], MoS_2/WSe_2 [17,18], MoS_2/$MoTe_2$ [19], and Sb_2Te_3/MoS_2 [20], have been successfully demonstrated and shown great potential in applications in future integrated electronic and optoelectronic fields [21–24]. Moreover, the atomically thin nature enables the flexible tuning of the charge carrier density in the components in p-n junctions by electrostatic means, which offers new avenues to design functions and improve the performances [25,26]. For example, Furchi *et al.* [23] reported atomically thin vdW p-n junction consisting of MoS_2 and WSe_2. Due to the ambipolar nature of WSe_2, the junction is tuned into n-n junction or p-n junction,

Key Laboratory for Micro-Nano Physics and Technology of Hunan Province, State Key Laboratory of Chemo/Biosensing and Chemometrics, College of Materials Science and Engineering, Hunan University, Changsha 410082, China
[†] These authors contributed equally to this work.
[*] Corresponding authors (emails: liidong@hnu.edu.cn (Li D); anlian.pan@hnu.edu.cn (Pan A))

 © Science China Press and Springer-Verlag GmbH Germany, part of Springer Nature 2020

with a rectification ratio of ~100 and photovoltaic response along with photoresponsivity of 11 mA W^{-1} at −1 V bias, and external quantum efficiency (EQE) less than 50%. Lee *et al.* [27] also reported the similar work, where the junction showed type tunable characteristics with maximum photoresponsivity of 120 mA W^{-1} and EQE of 34%. Additionally, Wang *et al.* [28] demonstrated the tunable GaTe-MoS_2 vdW p-n junction with a much improved device performances, such as high rectification ratio of 4×10^5, high photoresponsivity of 21.83 A W^{-1} and EQE of 61.68%. However, the photoresponsivity, response speed and EQE of 2D vdW p-n junction devices are still low, which may probably be attributed to the low light absorption efficiency. Cadmium sulfide (CdS) has been widely studied for its excellent optoelectronic properties and shows the potential to be produced in nanoscale in thickness [29]. The combination of CdS with 2D materials into heterostructures should be a feasible way to improve the optoelectronic properties of the heterostructures.

In this view, n-type CdS nanobelts (NBs) and p-type BP [9,30] were selected as components to fabricate the vdW p-n junctions. Electrical characterizations indicate that the heterostructure shows typical rectifying behavior (rectifying ratio up to 8×10^3), which can be further modulated by the outer electrical field applied on the gate. Interestingly, we have also observed anti-ambipolar behavior in the transfer curve. While under light illumination, excellent optoelectronic properties are observed. The optimized maximum photoresponsivity is measured to be 9.2×10^5 A W^{-1} at a low bias voltage of 1.0 V which is superior to those of reported p-n heterojunctions. Moreover, ultra-high specific detectivity (D^*) is deduced to be 3.2×10^{13} Jones. The device can also be operated at a self-powered mode, in which no drain bias is applied, while a high responsivity of 0.27 A W^{-1} and high EQE of 76% are collected. At the same time, the device also possesses fast response time (the rise time and decay time are about 13 and 5 ms). The CdS/BP heterojunction will find promising potential applications in future novel electronic and optoelectronics devices.

EXPERIMENTAL SECTION

Device fabrication

In the first step, CdS NBs were synthesized through a chemical vapor deposition (CVD) strategy, where a tube furnace (Kejing Materials Technology Co., Ltd., OTF-1200X) with a quartz tube (100 cm length, 45 mm inner diameter and 50 mm outer diameter) was used. An alumina boat with CdS powder (99.99%, Alfa Aesar) was located at the center of the furnace. Several silicon wafers with pre-sputtered Au films (10 nm thickness) were placed downstream of the gas flow, 15 cm far away from the furnace center. Before heating, the system was flushed with highly pure nitrogen for 40 min at a rate of 150 sccm. Then the furnace center temperature was ramped to 840°C with a rate of 14°C min^{-1}, under the pressure of 300 mbar. After maintaining the growth temperature for 60 min, the temperature was naturally reduced to room temperature. A silicon wafer covered with 300-nm-thick SiO_2 was employed as the substrate. The as-grown CdS NBs were transferred onto a 300-nm-thick SiO_2/p^+-Si substrate by a physical transfer method. BP flakes were then mechanically exfoliated onto the transparent polydimethylsiloxane (PDMS) and then transferred onto the desired CdS NB with the help of an optical microscope to form the heterojunction. Finally, the electrode patterns were defined by an electron beam lithography (EBL) and Au/Cr (60 nm/10 nm) metals were deposited by thermal evaporation, finally followed by a lift-off approach to produce the structures.

Characterizations

Photoluminescence (PL) spectroscopy and Raman spectra were characterized by a confocal microscopy (WITec, alpha-300) with the excitation laser of 400 nm. The device morphology was characterized by atomic force microscopy (AFM, Bruker Dimension Icon) in a tapping mode. The electrical measurement of the CdS/BP heterojunction was performed with an Agilent-B1500 semiconductor analyzer in a lakeshore vacuum chamber of 10^{-4} Pa. The optoelectronic properties were measured with a laser of 450 nm in a wavelength. We measured the power of light by an optical power meter and calculated the incident light power on the devices according to their area.

RESULTS AND DISCUSSION

A schematic configuration of the fabricated device is shown in Fig. 1a. The CdS NBs were firstly grown by the CVD approach, and then transferred onto a SiO_2/Si substrate. BP flakes were exfoliated onto a PDMS film though a mechanical exfoliation method. The BP flake was precisely aligned on the CdS NB (details of the device fabrication process can be seen in Fig. S1). Fig. 1b illustrates an optical image of a typical produced CdS/BP heterojunction device. The Raman spectra of the BP flake is shown in Fig. 1c. Three Raman peaks are collected in the BP flake, which are at 357, 434.8 and 462.6 cm^{-1}, corresponding to the A_g^1, B_{2g} and A_g^2 peaks, respectively

 © Science China Press and Springer-Verlag GmbH Germany, part of Springer Nature 2020

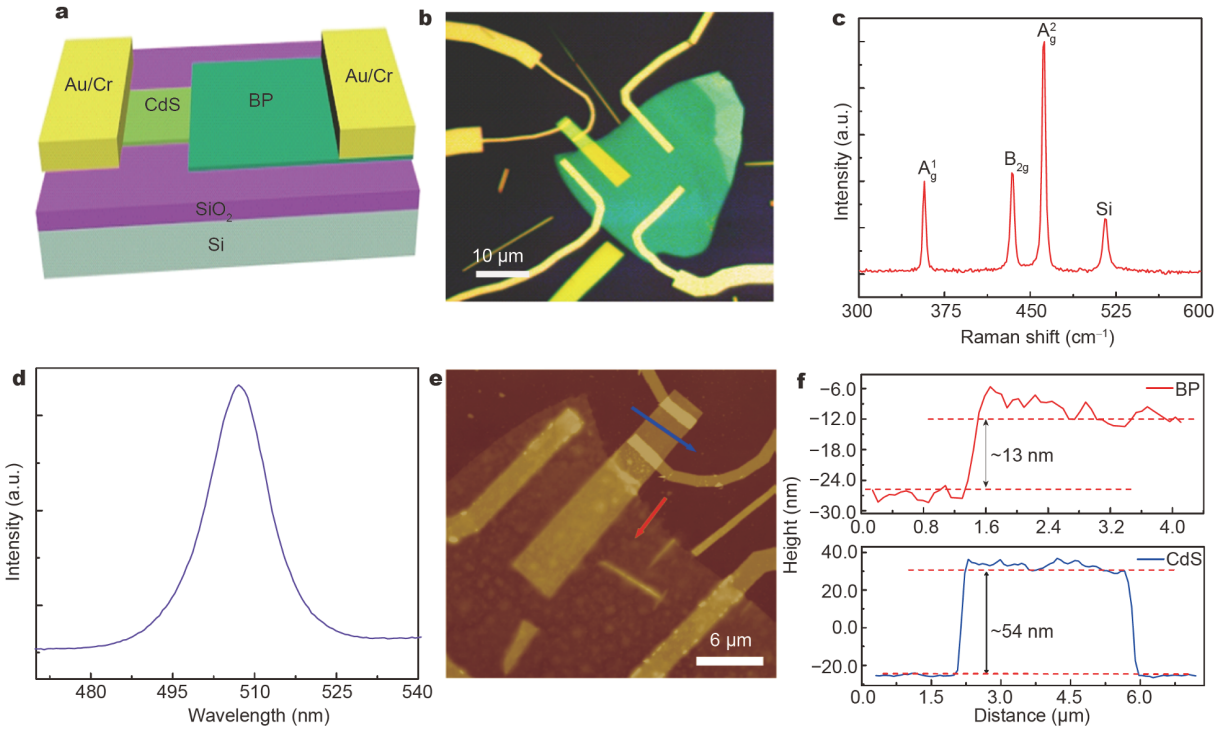

Figure 1 (a) Schematic device structure of the CdS/BP p-n heterojunction. (b) Optical image of a fabricated CdS/BP p-n heterojunction device. (c) Raman spectra of the BP flake. (d) PL spectra of the CdS NB. (e) AFM image of CdS and BP. (f) Height profiles corresponding to different parts marked in (e).

[31]. Fig. 1d depicts the PL spectra of the CdS NB, where an evident single emission peak at 507 nm is observed [32]. The AFM was used to characterize the heterostructure and the results are shown in Fig. 1e, f. It indicates that BP and CdS possess thickness of 13 and 54 nm, respectively.

The electrical properties of the CdS/BP vdW heterostructure devices were measured at room temperature in vacuum. Fig. 2a depicts the transfer characteristic of the CdS NB at different back gate voltages (V_{bg}), where Si is used as the gate electrode. It can be seen that the CdS field effect transistor (FET) exhibits typical n-type behavior. When the gate voltage is swept from −60 to +60 V, the channel drain current (I_{ds}) increases drastically from 10^{-12} to 10^{-6} A, with current on/off ratio exceeding 10^6. Fig. 2b shows the output characteristics of the CdS NB FET. The current is almost symmetric dependent on the bias voltages, indicating that the Au/Cr electrodes make good contact with the CdS. Fig. 2c shows the transfer characteristics (I_{ds}-V_{bg}) of pure BP flake by sweeping the gate bias from −60 to 60 V at different drain voltage (V_{ds}) values. The drain current first decreases to a minimum point at the gate voltage around 15 V and then goes up gradually, indicating ambipolar conduction behaviors, where both holes and electrons can be effectively induced by electrostatic doping. The device exhibits an on/off ratio of nearly 8×10^3 for the hole region and near 10^1 for the electron region. The relatively low on/off ratio for electron is due to the p-type doping nature of BP. The field effect mobility is estimated in the order of 162 $cm^2\ V^{-1}\ s^{-1}$ [33]. Fig. 2d shows the output curves of BP flake under different gate voltages. The I_{ds}-V_{ds} curves are linearly symmetric, indicating that the Au/Cr electrodes also make good contact with the BP flake. Fig. 2e shows the I_{ds}-V_{ds} characteristics of the CdS/BP heterojunction at V_{bg}=0 V. The observed *I-V* curve presents high rectification ratio over 8×10^3 with small bias voltage range of ±1 V. This curve can also be fitted by Shockley diode equation extended to include a series resistance R_s [34,35]:

$$I_{ds} = \frac{nV_T}{R_s} W\left[\frac{I_0 R_s}{nV_T}\exp\left(\frac{V_{ds}+I_0R_s}{nV_T}\right)\right] - I_0, \quad (1)$$

where V_T=K_BT/q is the thermal energy at temperature T, K_B is the Boltzmann constant, q is the electron charge, n is the ideality factor (n=1, p-n diode is ideal) and I_0 is the

 © Science China Press and Springer-Verlag GmbH Germany, part of Springer Nature 2020

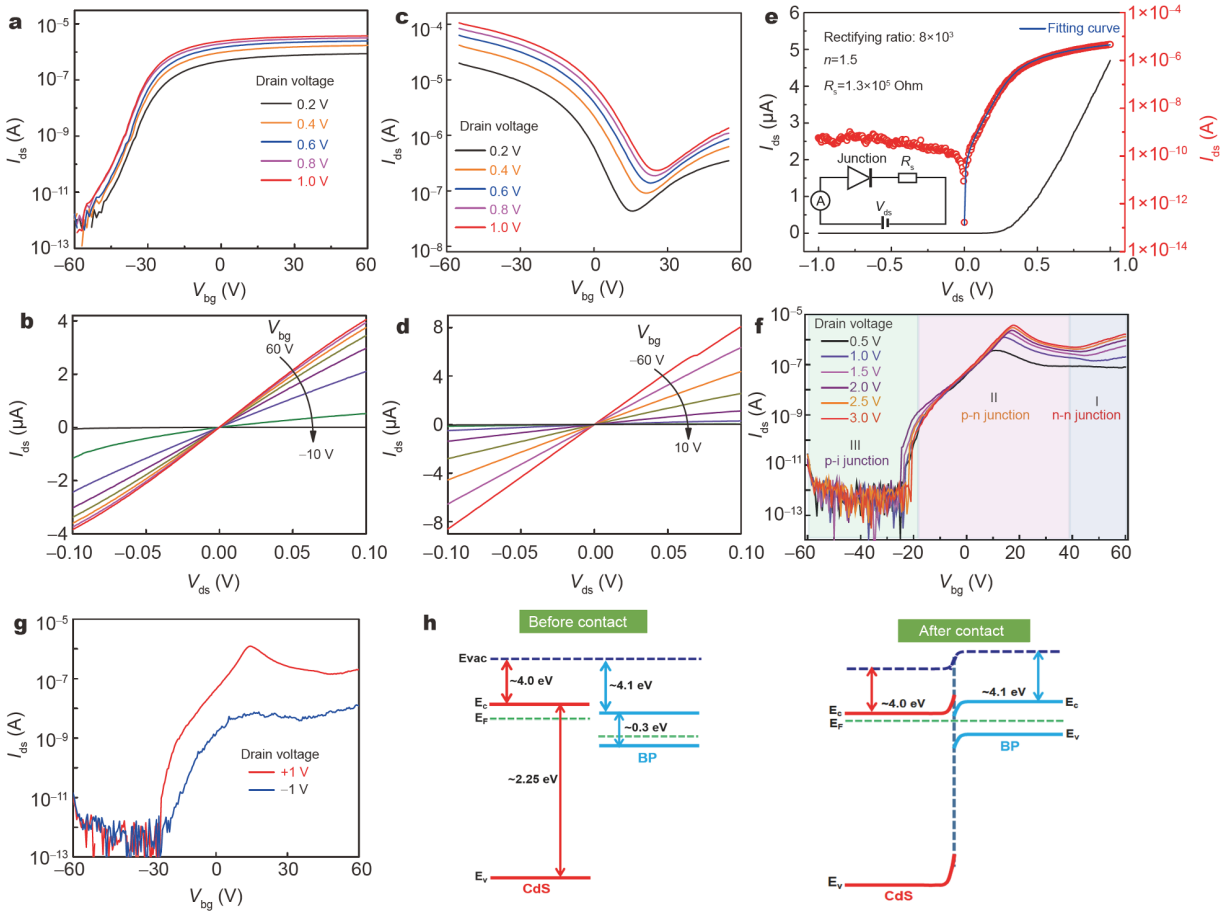

Figure 2 Electrical properties of the CdS/BP heterojunction. (a) Transfer curves of the CdS NB FET with Au/Cr electrodes. (b) Linear scale output curves of the CdS NB at various gate voltages. (c) I_{ds}-V_{bg} transfer curves of the BP FET at various drain voltages on semilog scale. (d) I_{ds}-V_{ds} output curves of BP at various gate voltages. (e) I_{ds}-V_{ds} characteristics curves of the CdS/BP heterojunction with V_{bg}=0 V on linear and semilog scale. (f) I_{ds}-V_{bg} transfer curves of the CdS/BP heterojunction device under different drain voltages. (g) Transfer curves of the CdS-BP heterojunction device with V_{ds} of +1 and −1 V. (h) Energy band diagram of the CdS-BP heterojunction before and after contact, ΔE, E_c, E_v, E_F and E_{vac} are band offset, conduction, valance level, Fermi energy and vacuum level.

saturation current. The inset image in Fig. 2e exhibits the equivalent circuit for Equation (1). By fitting the I_{ds}-V_{ds} curve, we can get that the n is 1.5 and R_s is 1.3×10^5 Ω. Here the contact resistance is mainly contributed by the metal-semiconductor contacts, the series BP region and the series CdS region. The gate dependent I-V curves are shown in Fig. S2. Fig. 2f plots the transfer characteristics of the device with drain bias ranging from 0.5 to 3.0 V. The transfer characteristics under different negative V_{ds} values are illustrated in Fig. S3. It is clear that the device shows electrically tunable gate voltage-dependent electronic properties. The I_{ds}-V_{bg} curves can be divided into three regions: n-n junction, p-n junction and p-i junction. In region I (V_{bg}>38 V), the heterojunction is fully turned on and the large I_{ds} current is dominated by the high electron concentration in both BP and CdS. In region II (−19 V<V_{bg}<+39 V), BP is p-doped and CdS remains n-type. As a result, p-n junction is formed at the interface with typical rectifying behavior (Fig. 2g). While the gate voltage is smaller than −19 V, the device shows very large output resistance, which can reasonably be attributed to that the CdS channel is fully depleted. Moreover, it can be seen that under negative bias voltage the heterojunction shows unipolar (n-type) behavior, whereas under positive bias the device shows antibipolar behavior. Such novel transport behavior can be reasonably understood with a simplified resistance model shown in Fig. S4. The energy band diagram of the CdS-BP heterojunction before and

 © Science China Press and Springer-Verlag GmbH Germany, part of Springer Nature 2020

after contact is shown in Fig. 2h. For the few-layer BP, the electron affinity is around 4.1 eV and it possesses small band gap of around 0.3 eV [36]. For the CdS NB, the corresponding values are around 4.0 and 2.25 eV [29], respectively. Therefore, a type-I (straddling) band alignment heterojunction is formed between CdS and BP. Under different bias, the energy bands are bent, leading to the formation of a potential barrier at the interface and charge carrier density of the junction can be modulated.

Fig. 3a shows the I_{ds}-V_{ds} curves under incident laser of 450 nm with power varied from 0.085 to 7.30 nW μm^{-2}, where obvious photovoltaic response is observed. A very clear open circuit voltage (V_{OC}) of 0.027 V and short circuit current (I_{SC}) of 0.04 μA are generated at a power density of 7.30 nW μm^{-2}. The small V_{OC} value can be attributed to the small Fermi level difference between CdS and BP. In addition, the produced electrical power (P_{el}) of the p-n junction can be evaluated by using the equation of $P_{el}=I_{ds}V_{ds}$. Fig. 3b plots the electrical power as a function of V_{ds} under various illumination power intensities. The maximum electrical power P_{el}=300 pW is obtained at a bias voltage of 15 mV with a power intensity of 7.30 nW μm^{-2}. Fig. 3c presents the variations of V_{OC} and I_{SC} with the incident laser power. Based on the equation of fill factor FF=$P_{el,m}/V_{oc}I_{sc}$, we can further get that the FF of the device is 0.27 for 7.30 nW μm^{-2}. Additionally, we measured the photovoltaic response of the device at the back gate voltage of 5 V as shown in Fig. S5. By increasing the laser power, it can be seen that both I_{SC} and V_{OC} are increased. Fig. 3d, f show the time domain V_{OC} switching behavior of the CdS/BP heterojunction using 450 nm illumination laser with different power intensities. As can

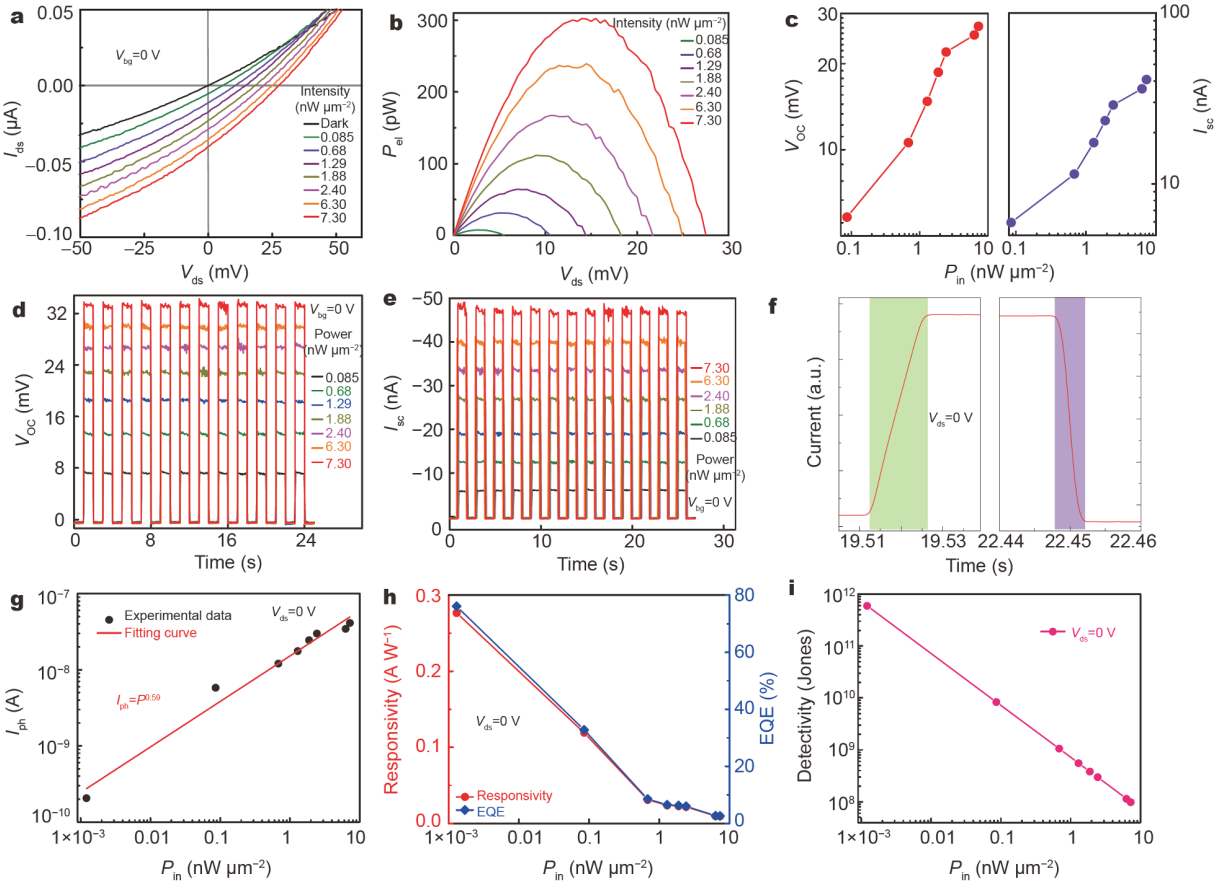

Figure 3 Photovoltaic properties of the CdS-BP vdW heterojunction. (a) I_{ds}-V_{ds} characteristics of the CdS/BP heterojunction under 450 nm laser with different power intensities at low bias voltage to investigate its photovoltaic effect. (b) Generated output electrical power (defined as $P_{el}=I_{ds}V_{ds}$ in the heterojunction as a function of V_{ds} under different power intensities. (c) The calculated I_{sc} and V_{oc} as a function of the power intensity. (d) Temporal response by photoswitching behavior, open circuit voltage V_{oc} as a function of time. (e) Temporal I_{sc} response of the device under laser switching on and off at V_{ds}=0 V, V_{bg}=0 V. (f) The time-resolved photoresponse exhibits fast photoswitching with a rise time and decay time of about 13 and 5 ms, respectively. (g) Photocurrent as a function of the various power intensities at V_{ds}=0 V. (h, i) Power-dependent photoresponsivity, EQE and photodetectivity at a zero bias.

© Science China Press and Springer-Verlag GmbH Germany, part of Springer Nature 2020

be seen, V_{OC} and I_{SC} changes periodically by switching the laser on and off, indicating high stability. Fig. 3f shows the temporal photocurrent response of the device. It is observed that the rise time and decay time are about 13 and 5 ms, respectively. Fig. 3g shows the extracted photocurrent ($I_{ph}=I_{light}-I_{dark}$) at different power intensities. The dependence between I_{ph} and power density can be expressed by the law $I_{ph}=P^{\alpha}$ [18,37], where α is calculated to be 0.59. Based on the I_{ph}, we can also get the photoresponsivity of the device, which can be expressed by $R=I_{ph}/PA$, where P is the light power density and A is the effective illumination area of the device. As shown in Fig. 3h, the largest responsivity of 0.27 A W^{-1} is obtained at incident light power of 0.0013 nW μm^{-2}. The EQE is defined as the ratio of the number of the collected charge carriers to the number of incident photons and can be calculated by EQE=$hcR/e\lambda$, where h, c, e, λ are the Planks constant, the speed of light, the electron charge and the wavelength of the incident light, respectively. The obtained EQE is as high as 76% at low incident power density, indicating that both the absorption efficiency and the photo-excited charge carrier separation efficiency of the device are very high [18,38]. These behaviors indicate that the CdS-BP heterojunction has promising potential for high performance self-powered photodetectors and solar energy harvesting.

Fig. 4a exhibits the I-V curves of the CdS/BP heterojunction under emission light of 450 nm. With increasing laser power intensity, more electron-hole pairs are generated and separated by the p-n junction, resulting in the gradual increase of the photocurrent. We also extracted the photocurrent at both forward bias condition and reverse bias condition, and the results are shown in Fig. 4b. The heterojunction shows larger photocurrent in forward bias voltages due to the larger forward dark current and high photoconductive properties. Another key parameter to quantify the photoresponse property for photodetector is the specific detectivity as shown in Fig. 4c. Assuming that the shot noise from the dark current is the major contributor to the limiting D^*, given by $D^*=RA^{1/2}(2eI_d)^{-1/2}$, where R is the responsivity, A is the effective area of the device, e is elementary charge and I_d is the dark current. The maximum obtained D^* is 1.68×10^{13} Jones at a bias of 1.0 V and weak power intensity of 0.0013 nW μm^{-2}, this value is higher than previously reported MoS_2/glassy-Gr [39], and AsP/InSe [40]. Fig. 4d shows the photoresponsivity of the device at different bias conditions. Maximum responsivity of 10^6 A W^{-1} is obtained at a low

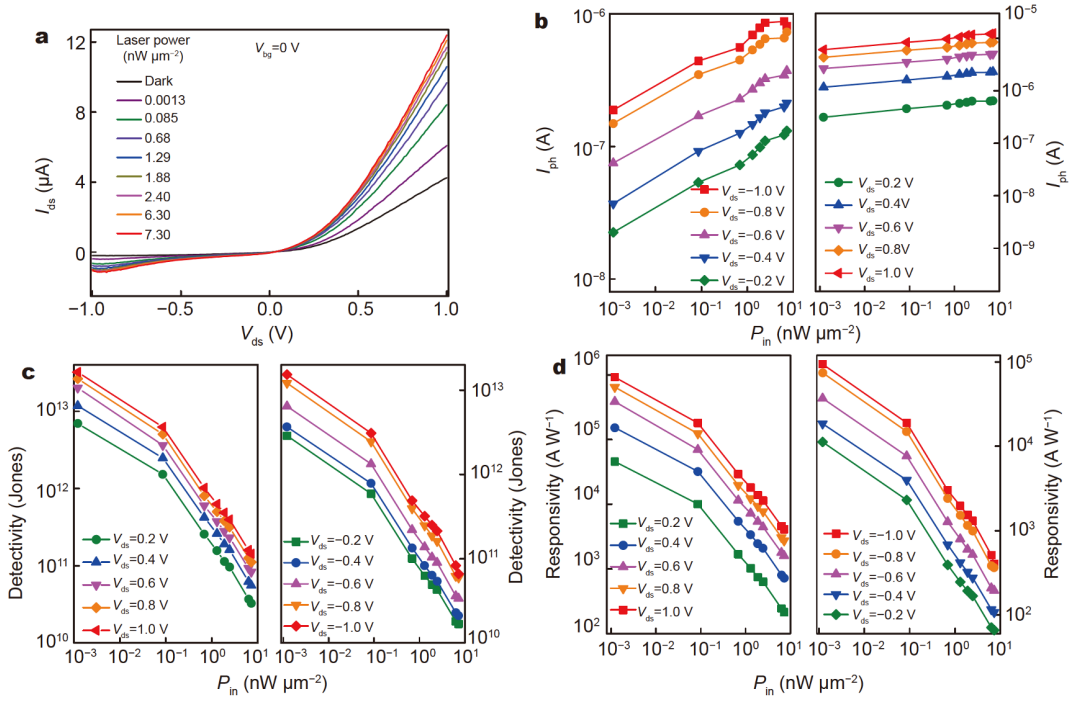

Figure 4 Optoelectronic characterization of the CdS/BP heterojunction. (a) I_{ds}-V_{ds} curves of the CdS/BP heterojunction under 450 nm laser in dark with various power intensities in linear scale. (b) Photocurrent as a function of the illumination power intensity at various V_{ds} values. (c) Specific detectivities of the CdS/BP heterojunction are plotted as a function of the laser power intensity at different V_{ds}. (d) The plots of photoresponsivities as a function of the laser power intensity at different V_{ds}.

 © Science China Press and Springer-Verlag GmbH Germany, part of Springer Nature 2020

bias voltage of 1.0 V and weak power intensity of 0.0013 nW μm^{-2}, which is much higher than those of reported heterojunctions [41,42]. Fig. S6 summarizes the performances of different 2D materials (photoresponsivity) under self-powered and bias voltage mode, respectively. The comparisons of figure of merit with the other 2D vdW heterojunctions are displayed in Table S1. These results suggest that the CdS/BP vdW p-n junction exhibits strong potential applications for the next-generation electronic and optoelectronic devices.

CONCLUSIONS

In conclusion, vertically stacked vdW CdS/BP p-n heterojunctions have been constructed. The electrical conductance of the achieved junctions can be tuned among n-n, p-n, and p-i types. The photoresponse properties under different biases and various power intensities were well investigated. The heterojunction can exhibit a record high photoresponsivity of 9.2×10^5 A W^{-1} and an ultrahigh specific detectivity of 3.2×10^{13} Jones at a low bias voltage of 1.0 V. In addition, the vertical CdS/BP p-n photodiode can also perform well at the self-powered mode due to the significant photovoltaic effect. These CdS/BP vdW heterojunctions with excellent performances will find a wide range of potential applications in integrated electronic and optoelectronic devices and systems.

Received 29 February 2020; accepted 13 April 2020; published online 23 June 2020

1 Wang QH, Kalantar-Zadeh K, Kis A, *et al.* Electronics and optoelectronics of two-dimensional transition metal dichalcogenides. Nat Nanotech, 2012, 7: 699–712
2 Novoselov KS, Geim AK, Morozov SV, *et al.* Electric field effect in atomically thin carbon films. Science, 2004, 306: 666–669
3 Duan X, Wang C, Shaw JC, *et al.* Lateral epitaxial growth of two-dimensional layered semiconductor heterojunctions. Nat Nanotech, 2014, 9: 1024–1030
4 Yang T, Zheng B, Wang Z, *et al.* Van der Waals epitaxial growth and optoelectronics of large-scale WSe_2/SnS_2 vertical bilayer p-n junctions. Nat Commun, 2017, 8: 1906
5 Li D, Zhu C, Liu H, *et al.* Light-triggered two-dimensional lateral homogeneous p-n diodes for opto-electrical interconnection circuits. Sci Bull, 2019, 65: 293–299
6 Buscema M, Groenendijk DJ, Steele GA, *et al.* Photovoltaic effect in few-layer black phosphorus PN junctions defined by local electrostatic gating. Nat Commun, 2014, 5: 4651
7 Cui F, Feng Q, Hong J, *et al.* Synthesis of large-size 1T' $ReS_{2x}Se_{2(1-x)}$ alloy monolayer with tunable bandgap and carrier type. Adv Mater, 2017, 29: 1705015
8 Gong C, Zhang Y, Chen W, *et al.* Electronic and optoelectronic applications based on 2D novel anisotropic transition metal dichalcogenides. Adv Sci, 2017, 4: 1700231
9 Youngblood N, Chen C, Koester SJ, *et al.* Waveguide-integrated black phosphorus photodetector with high responsivity and low dark current. Nat Photon, 2015, 9: 247–252
10 Liu Y, Weiss NO, Duan X, *et al.* Van der Waals heterostructures and devices. Nat Rev Mater, 2016, 1: 16042
11 Wei Z, Li B, Xia C, *et al.* Various structures of 2D transition-metal dichalcogenides and their applications. Small Methods, 2018, 2: 1800094
12 Cao S, Xing Y, Han J, *et al.* Ultrahigh-photoresponsive UV photodetector based on a BP/ReS_2 heterostructure p-n diode. Nanoscale, 2018, 10: 16805–16811
13 Lv Q, Yan F, Wei X, *et al.* High-performance, self-driven photodetector based on graphene sandwiched $GaSe/WS_2$ heterojunction. Adv Opt Mater, 2018, 6: 1700490
14 Zhou X, Hu X, Zhou S, *et al.* Tunneling diode based on WSe_2/SnS_2 heterostructure incorporating high detectivity and responsivity. Adv Mater, 2018, 30: 1703286
15 Chen Y, Wang X, Wu G, *et al.* High-performance photovoltaic detector based on $MoTe_2/MoS_2$ van der Waals heterostructure. Small, 2018, 14: 1703293
16 Zheng W, Feng W, Zhang X, *et al.* Anisotropic growth of non-layered CdS on MoS_2 monolayer for functional vertical heterostructures. Adv Funct Mater, 2016, 26: 2648–2654
17 Sun M, Fang Q, Xie D, *et al.* Novel transfer behaviors in 2D MoS_2/WSe_2 heterotransistor and its applications in visible-near infrared photodetection. Adv Electron Mater, 2017, 3: 1600502
18 Huo N, Kang J, Wei Z, *et al.* Novel and enhanced optoelectronic performances of multilayer MoS_2-WS_2 heterostructure transistors. Adv Funct Mater, 2014, 24: 7025–7031
19 Duong NT, Lee J, Bang S, *et al.* Modulating the functions of $MoS_2/MoTe_2$ van der Waals heterostructure *via* thickness variation. ACS Nano, 2019, 13: 4478–4485
20 Liu H, Li D, Ma C, *et al.* Van der Waals epitaxial growth of vertically stacked Sb_2Te_3/MoS_2 p-n heterojunctions for high performance optoelectronics. Nano Energy, 2019, 59: 66–74
21 Baugher BWH, Churchill HOH, Yang Y, *et al.* Optoelectronic devices based on electrically tunable p-n diodes in a monolayer dichalcogenide. Nat Nanotech, 2014, 9: 262–267
22 Li D, Chen M, Sun Z, *et al.* Two-dimensional non-volatile programmable p-n junctions. Nat Nanotech, 2017, 12: 901–906
23 Furchi MM, Pospischil A, Libisch F, *et al.* Photovoltaic effect in an electrically tunable van der Waals heterojunction. Nano Lett, 2014, 14: 4785–4791
24 Zhu C, Sun X, Liu H, *et al.* Nonvolatile $MoTe_2$ p-n diodes for optoelectronic logics. ACS Nano, 2019, 13: 7216–7222
25 Kwak DH, Jeong MH, Ra HS, *et al.* Lateral WSe_2 p-n junction device electrically controlled by a single-gate electrode. Adv Opt Mater, 2019, 7: 1900051
26 Li D, Wang B, Chen M, *et al.* Gate-controlled BP-WSe_2 heterojunction diode for logic rectifiers and logic optoelectronics. Small, 2017, 13: 1603726
27 Lee CH, Lee GH, van der Zande AM, *et al.* Atomically thin p-n junctions with van der Waals heterointerfaces. Nat Nanotech, 2014, 9: 676–681
28 Wang F, Wang Z, Xu K, *et al.* Tunable GaTe-MoS_2 van der Waals p-n junctions with novel optoelectronic performance. Nano Lett, 2015, 15: 7558–7566
29 Guo P, Hu W, Zhang Q, *et al.* Semiconductor alloy nanoribbon lateral heterostructures for high-performance photodetectors. Adv Mater, 2014, 26: 2844–2849

 © Science China Press and Springer-Verlag GmbH Germany, part of Springer Nature 2020

30 Gehring P, Urcuyo R, Duong DL, *et al.* Thin-layer black phosphorus/GaAs heterojunction p-n diodes. Appl Phys Lett, 2015, 106: 233110
31 Sugai S, Shirotani I. Raman and infrared reflection spectroscopy in black phosphorus. Solid State Commun, 1985, 53: 753–755
32 Li L, Lou Z, Shen G. Hierarchical CdS nanowires based rigid and flexible photodetectors with ultrahigh sensitivity. ACS Appl Mater Interfaces, 2015, 7: 23507–23514
33 Li L, Yu Y, Ye GJ, *et al.* Black phosphorus field-effect transistors. Nat Nanotech, 2014, 9: 372–377
34 Banwell TC, Jayakumar A. Exact analytical solution for current flow through diode with series resistance. Electron Lett, 2000, 36: 291–292
35 Sah C, Noyce R, Shockley W. Carrier generation and recombination in P-N junctions and P-N junction characteristics. Proc IRE, 1957, 45: 1228–1243
36 Perello DJ, Chae SH, Song S, *et al.* High-performance n-type black phosphorus transistors with type control *via* thickness and contact-metal engineering. Nat Commun, 2015, 6: 7809
37 Wei X, Yan F, Lv Q, *et al.* Fast gate-tunable photodetection in the graphene sandwiched WSe_2/GaSe heterojunctions. Nanoscale, 2017, 9: 8388–8392
38 Wang P, Liu S, Luo W, *et al.* Arrayed van der Waals broadband detectors for dual-band detection. Adv Mater, 2017, 29: 1604439
39 Xu H, Han X, Dai X, *et al.* High detectivity and transparent few-layer MoS_2/glassy-graphene heterostructure photodetectors. Adv Mater, 2018, 30: 1706561
40 Wu F, Xia H, Sun H, *et al.* AsP/InSe van der Waals tunneling heterojunctions with ultrahigh reverse rectification ratio and high photosensitivity. Adv Funct Mater, 2019, 29: 1900314
41 Kufer D, Nikitskiy I, Lasanta T, *et al.* Hybrid 2D-0D MoS_2-PbS quantum dot photodetectors. Adv Mater, 2015, 27: 176–180
42 Pezeshki A, Shokouh SHH, Nazari T, *et al.* Electric and photovoltaic behavior of a few-layer α-$MoTe_2$/MoS_2 dichalcogenide heterojunction. Adv Mater, 2016, 28: 3216–3222

Acknowledgements This work was supported by the National Natural Science Foundation of China (U19A2090, 51902098, 51972105, 51525202 and 61574054), and Hunan Provincial Natural Science Foundation of China (2018RS3051).

Author contributions Zubair M, Zhu C, Li D and Pan A designed and performed the experiments, and wrote the manuscript. Zhu C, Sun X and Yi J advised on data analysis. Liu H synthesized the CdS flakes. Zhu X, Li D and Pan A analyzed the results, and provided theoretical guidance. All authors contributed to the general discussion.

Conflict of interest The authors declare that they have no conflict of interest.

Supplementary information Supporting data are available in the online version of the paper.

Muhammad Zubair is a PhD researcher at the College of Materials Science and Engineering in Hunan University. His research focuses on the fabrication of low dimensional semiconductor materials-based van der Waals heterostructures and their applications in electronics and optoelectronics.

Chenguang Zhu is currently a PhD candidate at the College of Materials Science and Engineering, Hunan University. His research interests mainly include the fabrication of nanodevices, the performance and application of kinds of semiconductor materials.

Xingxia Sun is currently a PhD candidate at the College of Materials Science and Engineering, Hunan University. Her main research interests include the synthesis of nanomaterials with controlled CVD route, and their applications in photoelectric devices.

Dong Li received his BSc degree in 2013 and PhD degrees in 2018 from the School of Physical Science and Engineering, Tongji University. Afterwards, he joined the Key Laboratory for MicroNano Physics and Technology of Hunan Province in Hunan University as a professor. His research interests include low-dimensional materials, devices and their applications in future electronics and optoelectronics.

Anlian Pan received his PhD degree from the Institute of Physics, Chinese Academy of Sciences in 2006. Afterwards, he worked for one year as a Humboldt Research Fellow with Prof. Ulrich Goesele at Max Planck Institute of Microstructure Physics, and then joined Arizona State University as a Postdoctoral Fellow, where he became a research assistant professor. He came back to Hunan University in 2010 and has been working as the distinguished professor of "Furong" scholar in Hunan province since then. His research interests include the micro-nano optical, electronics of semiconductor nanostructures.

 © Science China Press and Springer-Verlag GmbH Germany, part of Springer Nature 2020

基于硫化镉-黑磷范德华异质结的超高响应光电二极管

Muhammad Zubair[†], 朱晨光[†], 孙兴霞[†], 刘华伟, 郑弼元, 易佳丽, 朱小莉, 李东[*], 潘安练[*]

摘要 近年来二维材料因其超薄的厚度及新颖的电、光及光电特性受到了广泛关注. 此外, 二维材料表面无悬挂键, 这使得其可以直接通过范德华力相互结合形成范德华异质结, 为构建具有优异性能的新型器件提供了新的机遇. 本文采用范德华集成方法将n型硫化镉和p型黑磷垂直堆垛起来构筑了p-n结二极管. 输运特性测试表明, 该p-n结器件表现出高的整流比(8×10^3)和低的理想因子(1.5). 同时, 在光照下器件表现出超高的光响应度和比探测率, 分别可达9.2×10^5 A W^{-1}和3.2×10^{13} Jones, 与目前所报道的二维异质结光电探测的最高水平相当. 当器件工作于自驱动探测模式时, 仍表现出极好的光探测性能, 光响应度和响应速度分别可达0.27 A W^{-1}和~10 ms. 所制备的硫化镉/黑磷异质结器件将会在新一代纳米电子、光电子器件中扮演重要角色.

 © Science China Press and Springer-Verlag GmbH Germany, part of Springer Nature 2020